The Influence of Freshwater Biofilms on Drag in Hydroelectric Power Schemes

J.M. ANDREWARTHA[1], J.E. SARGISON[1], K.J. PERKINS[2]
[1] School of Engineering, [2] School of Plant Science
University of Tasmania
Churchill Avenue, Sandy Bay, Hobart, Tasmania
AUSTRALIA
Jessica.Andrewartha@utas.edu.au http://www.eng.utas.edu.au

Abstract: - Freshwater biofilms are currently being studied to determine their effect on the capacity of hydroelectric power scheme canals and the structure of their turbulent wall layers. Mean velocity boundary layer profiles and total drag measurements have been conducted in a purpose built recirculating water tunnel on freshwater biofilms grown in a hydroelectric canal. Two different fouled surfaces were compared with a smooth painted surface to determine the effects of the physical characteristics of a biofilm on skin friction drag. A 310% increase in local skin friction coefficient was measured for a biofilm dominated by long filamentous algae streamers, and a 50% increase was measured for a biofilm dominated by a low-form gelatinous diatom.

Key-Words: - biofilm, biofouling, boundary layer, drag, hydroelectric, skin friction, water tunnel.

1 Introduction

Hydro Tasmania is a hydroelectric utility in Tasmania, Australia and operates 27 hydroelectric power stations with a total installed capacity of over 2500 MW. Water is supplied through an extensive water conveyance system including 170 km of canals and 60 km of pipelines. Extensive biofilm growth occurs on the internal surfaces of many of Hydro Tasmania's canals and pipelines causing significant reductions in capacity.

The detrimental effect of biofilms on skin friction is well established and the increases in frictional resistance and resultant energy losses due to biofilms are of concern to industry including hydroelectric power generators and ship owners [1, 2]. Much research has been done on the effect of biofilms on drag in the marine environment. Both full-scale ship trials [1] and laboratory studies [3, 4] have shown that the presence of biofilms can have a substantial detrimental effect on skin friction and hence ship performance.

Schultz and Swain [3] studied turbulent boundary layers over marine biofilms and found an increase in skin friction coefficient of 68% for a slime film and 190% for a surface dominated by filamentous green algae, when compared to a smooth surface. The results demonstrate the importance of low-form biofilms and the effect of biofilm morphology, thickness and composition on hydrodynamic drag.

Industrial experience has shown that the accumulation of biofilms in freshwater pipelines causes a measured increase in headloss and hence decreased generating efficiency and revenue for hydroelectric schemes [2, 5]. Likewise, the seasonal growth of photosynthesising algae combined with harsh weather conditions reduces the capacity in Hydro Tasmania's open canals and flumes.

The University of Tasmania (UTAS) and Hydro Tasmania are investigating the effects of biofouling and surface roughness in water conveyance structures. This paper presents results of a study of Tarraleah No.1 Canal, including a detailed boundary layer analysis conducted in a purpose-built laboratory facility.

2 Case Study

2.1 Tarraleah No.1 Canal

Tarraleah No.1 Canal is a 19 km long concrete-lined open channel which conveys water from Lake King William to the Tarraleah Power Station in central Tasmania. The Tarraleah Power Station has a 90 MW capacity, but due to long term water constraints caused by the decreased capacity of Tarraleah No.1 Canal, the station can only operate at 70 – 75 MW.

The current canal capacity is limited by degradation of the concrete surface and extensive biofilm growth. The average water velocity is approximately 2 m/s. The canal is drained and

scrubbed annually to remove as much of the biofilm mat from the concrete surface as possible. A recent field study found a 10% increase in capacity as a direct result of removing the biofilm mat from the surface of Tarraleah No.1 Canal, increasing the maximum capacity from 21.3 m^3/s in the fouled state to 23.4 m^3/s in the clean state [6].

The capacity of the canal varies considerably depending on the morphology, thickness and composition of the biofilm [3, 5]. The growth of fouling in Tarraleah No.1 Canal is seasonal, with more growth occurring over the warmer summer months.

2.2 Description of Fouling Species

A common fouling species in both marine and freshwater environments is the diatom. Diatoms are microscopic, single-celled algae and are commonly the first species to colonise a freshly submerged surface [7]. Diatoms attach themselves to the surface, which allows them to remain in areas where photosynthesis and nutrient access conditions are optimal [8].

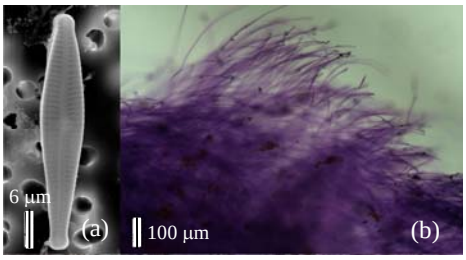

Fig. 1 (a) Single *Gomphonema* cell, (b) *Gomphonema* mucous stalks

The dominant diatom species in Tarraleah No. 1 Canal is *Gomphonema*, a raphid diatom with cells 35 μm long and 6 μm wide (Fig. 1a). *Gomphonema* secretes a mucous stalk which pushes the cells away from the wall (Fig. 1b) towards better light and nutrient conditions [9]. The stalks observed from the fouling at Tarraleah are hundreds of microns long, tens of times the size of the cell itself. As seen in Fig. 1b, stalking is intense and the bulk of the fouling seen on the canal wall is made up of stalk material. Debris, dead cells and other algal cells become trapped in the fouling, creating a dense mat.

Algae streamers up to 200 mm long have also been observed to grow in Tarraleah No.1 Canal, and it is expected that they will cause greater drag than the low-form gelatinous *Gomphonema*.

3 Laboratory Studies

3.1 Water Tunnel Set-Up

All experimental studies were completed in the UTAS Water Tunnel (Fig. 2), which was constructed specifically for the study of freshwater biofilms and has the capability to investigate a range of different surfaces including smooth painted, artificially roughened, and biological surfaces. Detailed descriptions of the water tunnel are given in Barton [5] and Barton *et al.* [10].

The working section was sized to replicate flow conditions in Tarraleah No.1 Canal and other Hydro Tasmania conduits, as given in Table 1. The working section is 2.2 x 0.6 x 0.2 m with 997 mm x 597 mm test plates suspended from the lid by 4 precision machined flexures to form the roof of the working section. A shear beam load cell (model MTI-4856-SB) was incorporated into the suspension of the test plate to allow the measurement of the total drag on the installed test plate [5, 10]. A flow conditioner, consisting of 2 sections of honeycomb and steel mesh, is installed upstream of the 2 m long contraction (contraction ratio = 3:1). The boundary layer is tripped upstream of the working section to ensure a turbulent boundary layer over the test plate. The freestream velocity in the working section ranges between 0.2 – 2.0 m/s. The water temperature is controlled by a cooling system and was set to 15 ± 0.5 ^oC for the duration of this study. The average water density was 999.0 kg/m^3 and the average water viscosity was 0.00114 kg/ms.

	R (m)	*U* (m/s)	*u** (m/s)
UTAS Water Tunnel	0.75	0-2	0.079-0.131
Tarraleah No.1 Canal	1.30	0-2	0.098

Table 1. Typical hydraulic conditions: water tunnel working section and Tarraleah No.1 Canal. (*R* = hydraulic radius, *U* = mean velocity, *u** = wall shear velocity).

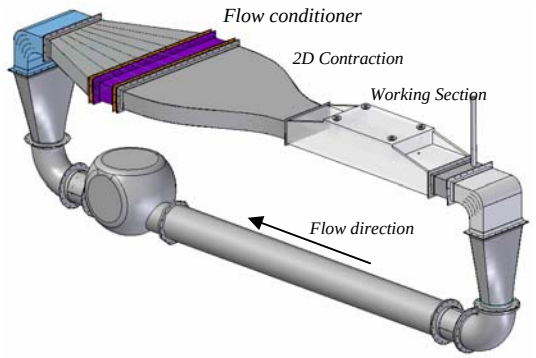

Fig. 2 UTAS Water Tunnel Schematic

3.2 Test Specimens

Three different test specimens were investigated: a smooth painted reference plate (SP), and two different fouled plates (FP1 and FP2). The test plates were constructed of 3 mm thick mild steel.

Racks are installed in Tarraleah No.1 Canal to allow the insertion of test plates into the canal with the aim to grow flow-conditioned biofilms. FP1 was placed in a high velocity section, whereas FP2 was placed in a low velocity section. The biofilm on FP1 consisted of a mat of *Gomphonema* and algae streamers up to 200 mm long, as shown in Fig. 3a. The fouling on FP1 is believed to be representative of the fouling in the canal (Fig. 3b). The biofilm on FP2 consisted of a low-form gelatinous biofilm, with no notable algae streamers (Fig. 3c).

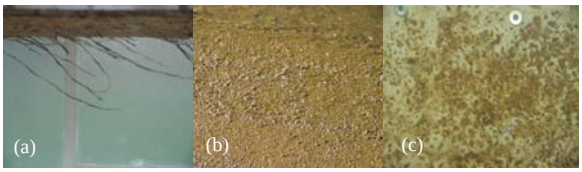

Fig. 3 (a) FP1 in water tunnel side view (no flow), algae streamers up to 200 mm long. (b) Fouled canal wall. (c) FP2 (low-form biofilm).

3.3 Experimental Procedure/Data Reduction

3.3.1. Boundary Layer Traverses

Mean velocity boundary layer traverses were completed 95 mm downstream from the leading edge of the test plate using a Pitot probe and static wall tapping connected to a Validyne variable reluctance differential pressure transducer (model DP15). The Pitot/static pressure differential was measured at 51 locations throughout the boundary layer on a logarithmic scale at a sampling rate of 1 kHz with the probe moved by an automatic linear actuator with a minimum step of 0.01 mm. All measurements were corrected for small temporal changes in test section velocity using the pressure differential across the contraction.

Two methods were used to determine the wall shear velocity, u^*, and the local skin friction coefficient, c_f. The Preston tube method [11] was used for SP boundary layer profiles and the results were corrected for the effects of a transverse velocity gradient deflecting the streamlines by using an apparent shift in location of the centre of the probe using the method proposed by McKeon *et al.* [12].

An adaptation of the Clauser chart method developed by Perry *et al.* [13] known as the log-law slope method was used for the fouled test plates, and has been used with success by other researchers [1, 3-5]. As it is difficult to determine the exact location of the wall for rough or fouled test plates, a wall origin error, ε, is introduced. The method forces a linear log-law region by adjusting ε in small increments until a linear regression line of best fit is determined for plots of u^+ versus $ln(y+\varepsilon)^+$ within the log law region (where $u^+ = u/u^*$, u = local velocity, $(y+\varepsilon)^+ = (y+\varepsilon)u^*/\nu$, y = location in boundary layer, and ν = kinematic viscosity).

The inner cut-off for the log-law region was set to 0.3 mm, and the outer cut-off was taken at 10% of the boundary layer thickness, δ [1, 5], where δ was based on the momentum thickness using power law relations (n = 7 SP, n = 5 FP1, FP2), as it is less sensitive to accurate wall origin.

The slope of the regression line of best fit of u/U vs $ln(yU/\nu)$ is used to determine c_f, as given by (1), where U = freestream velocity. The expression for u^* is given by (2), where κ is the von Karman constant and has the value of 0.41.

$$c_f = 2\kappa^2 (slope)^2 \tag{1}$$

$$u^* = U \Big/ \sqrt{2c_f^{-1}} \tag{2}$$

3.3.2. Total Drag Measurements

The force balance arrangement used to obtain total drag measurements is described in detail by Barton *et al.* [10]. Measurements were conducted at 1 kHz over a sampling time of 60 seconds.

The drag on a flat plate of width b and length l is given by (3), where ρ is the water density and C_D is the total drag coefficient. To compare experimental and theoretical results for an isolated plate, it is necessary to allow for the non-zero boundary layer thickness at the test plate leading edge. This is achieved by estimating a virtual origin at distance l_1 upstream which would produce the same boundary layer thickness at the leading edge (see Fig. 4).

Based on the boundary layer thickness derived from the mean velocity boundary layer traverses, the value of l_1 can be determined using (4) which is based on the $1/7^{th}$ power law, where $Re_l = Ul/\nu$. The theoretical drag on the test plate can then be obtained by (5) and (6). The equivalent sandgrain roughness, k_s, can be determined by (7), as suggested by Schlichting [14].

$$Drag = C_D \rho blU^2 / 2 \quad (3)$$

$$l_1 = \delta \mathrm{Re}_{l_1}^{0.167} / 0.22 \quad (4)$$

$$C_D = 0.074 / \mathrm{Re}_l^{\frac{1}{5}} \quad (5)$$

$$Drag = C_{D(l_2)} \rho bl_2 U^2 / 2 - C_{D(l_1)} \rho bl_1 U^2 / 2 \quad (6)$$

$$C_D = \left(1.89 + 1.62 \log(l / k_s)\right)^{-2.5} \quad (7)$$

$$\frac{u}{u^*} = \frac{1}{\kappa} \ln\left(\frac{y+\varepsilon}{k_s}\right) + C \quad (8)$$

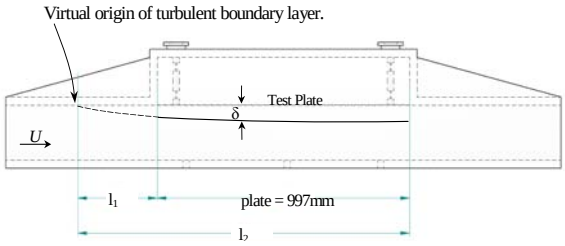

Fig. 4 Assumed boundary layer development over the test plate.

3.4 Uncertainty Analysis

The uncertainty in the velocity was determined using repeatability tests for a smooth test plate. Ten replicate velocity traces were taken at 5 mm from the wall and in the freestream. In order to determine the 95% confidence interval for a single statistic, the standard deviation was multiplied by the two-tailed t value (t = 2.262) for 9 degrees of freedom [3, 15, 16]. Mean velocity measurements in the near wall region attract a higher level of uncertainty due to the intrusive nature of the Pitot probe, with an uncertainty of ± 0.7% in the near wall region compared to ± 0.1% in the freestream. Water temperature was measured to an accuracy of 0.5°C. The uncertainty in c_f was determined using sequential perturbation analysis and found to be less than 1% for the Preston tube method, and ± 9.5% for the log-law slope method. Barton *et al.* [10] gives an uncertainty of ± 2.7% (with 95% confidence) in total drag coefficient C_D, determined from the total drag measurements.

3.5 Boundary Layer Parameters

A summary of the main boundary layer parameters for each test plate is given in Table 1 (where θ is the momentum thickness and Δu^+ is the roughness function). For hydraulically rough flow k_s can be determined using (8), where C = 8.5 for the case of Nikuradse's sand (geometrically similar roughness elements). It is recognised that a single parameter, such as a roughness height, does not adequately describe a compliant surface such as a biofilm [3-5]. However, a series of parameters that successfully relate the biofilm to the roughness function are yet to be formulated. Fig. 5 compares the local skin friction coefficient, c_f, for smooth and fouled test plates.

	Re_θ	U (m/s)	θ (mm)	C_f	ε (mm)	k_s (mm)	Δu^+
SP	3650	1.33	3.11	0.0036	-	-	-
SP	4610	1.55	3.40	0.0034	-	-	-
SP	4480	1.63	3.15	0.0035	-	-	-
SP	5150	1.74	3.36	0.0034	-	-	-
SP	5380	1.88	3.26	0.0034	-	-	-
FP1	4250	1.35	3.59	0.0141	0.67	5.6	11.9
FP1	4820	1.57	3.46	0.0122	0.71	4.2	11.4
FP1	5210	1.79	3.30	0.0154	0.88	6.1	12.9
FP2	4800	1.57	3.47	0.0051	0.23	0.2	3.5
FP2	5490	1.80	3.49	0.0051	0.18	0.2	3.7
FP2	5980	1.96	3.45	0.0050	0.14	0.3	3.9

Table 2. Boundary layer parameters.

3.6 Mean Velocity Profiles

Boundary layer mean velocity profiles for all test plates are presented in Fig. 6. The results shown are for a range of Reynolds numbers and normalised by u^*. The Log Law was fitted to the smooth plate velocity profiles using (9), where the smooth wall log law constant, B, was taken as 5.0. The Log Law can be modified for rough surfaces by subtracting the roughness function, Δu^+, which represents the shift from the smooth wall profile.

$$u^+ = \frac{1}{\kappa} \ln y^+ + B \quad (9)$$

3.7 Total Drag Measurements

Fig. 7 compares the total drag coefficient data for SP and FP2 (data was not available for FP1). It is noted that the presence of the biofilm on the test plate has caused an increase in C_D. The average sandgrain roughness for FP2 was 0.57 mm, as derived from (7).

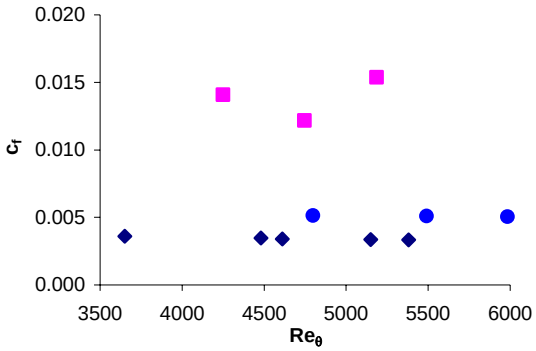

Fig. 5 Comparison of local skin friction coefficient data from mean velocity boundary layer traverses. ♦ SP, ■ FP1, ● FP2.

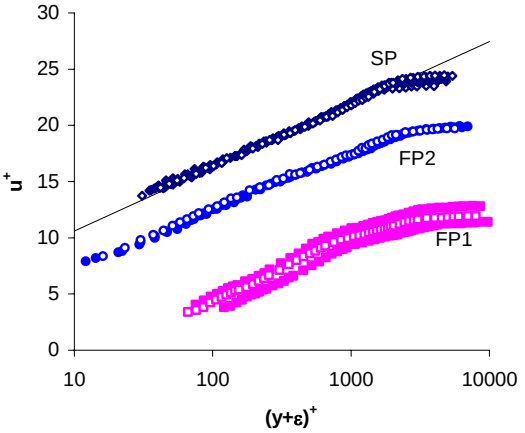

Fig. 6 Comparison of mean velocity boundary layer profiles normalised by u^*. ♦ SP, ■ FP1, ● FP2.

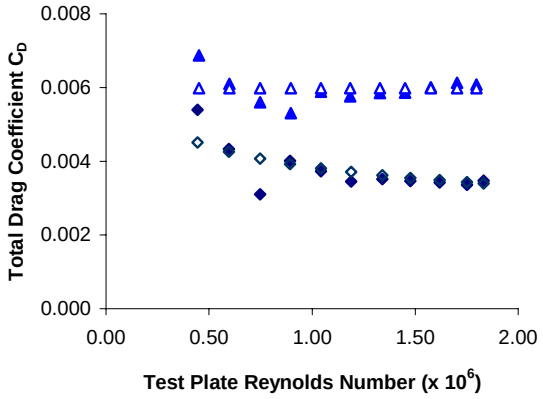

Fig. 7 Comparison of total drag coefficient data from total drag measurements. ♦ SP (exp) ◊ SP (theor) ▲ FP2 (exp) △ FP2 (theor)

4 Discussion

The two fouled plates used in this study were grown in the field in different locations, and hence had different physical characteristics. FP1 was grown in a high flow region and consisted of a dense mat of the low-form gelatinous *Gomphonema* and algae streamers up to 200mm long. FP1 (average c_f = 0.0139) exhibited a 310% increase in local skin friction coefficient over the smooth reference plate (average c_f = 0.0034), as illustrated in Fig. 5. FP2 (c_f = 0.0051) was grown in a lower velocity region and consisted of a low-form gelatinous biofilm with no algae streamers and exhibited a 50% increase in c_f over the smooth reference plate.

Likewise, in Fig. 6 the velocity profiles for FP2 are much closer to the smooth plate profile than FP1. The results are more scattered for FP1 which may be due to the motion of the algae filaments, or the higher degree of uncertainty due to the sensitivity of c_f to small changes in the wall origin error, ε, or the cut-offs for the log-law region. Both Schultz and Swain [3] and Lewthwaite *et al.* [1] report a larger uncertainty in results using the log-law slope method, mainly due to the introduction of two extra degrees of freedom in the analysis (ε and Δu^+).

The average total drag coefficient, C_D, was 0.0059 for FP2, a 60% increase over the results for SP (C_D = 0.0037).

The equivalent sandgrain roughness values obtained for the fouled plates provide an indication of the effective roughness of the biofilm. The average k_s value obtained for FP1 from the velocity profiles was 5.3mm. The k_s values obtained using the two different methods were slightly different for FP2, with k_s = 0.57 mm from the total drag measurements, and k_s = 0.25 mm from the velocity profiles. The velocity profile value represents the local k_s in the vicinity of the Pitot probe, whereas the total drag value provides an indication of the roughness condition of the entire test plate. It is widely recognised that the effective roughness caused by biofilm growth is considerably greater than the absolute thickness of the biofilm layer, due to the motion of the biofilm under flow conditions [2-5].

The roughness function, Δu^+, was found to be approximately 12.1 for FP1, and 3.7 for FP2. Future work will attempt to relate this roughness function to the characteristics of the biofilm.

Two mechanisms for energy dissipation were observed during the laboratory studies:

1. The algae filaments were observed to flutter in three dimensions under flow conditions. It is thought that this movement removes more momentum from the flow than low-form gelatinous biofilms [3].
2. The low-form gelatinous biofilms were also observed to vibrate under flow conditions.

The dense mat structure of the *Gomphonema* significantly impedes the flow in the near wall region, as the water is forced through the biofilm mat.

The results indicate that the drag exerted by a biofilm is a function of the physical characteristics of the biofilm. This assertion is supported in the literature [2-5, 7] with many authors concluding that the composition and morphology of the biofilm determines the hydrodynamic drag. For example Schultz and Swain [3] found an increase in c_f of 68% for a 350 μm thick slime film, compared to an increase of 190% for a 310 μm thick filamentous algae surface. In the present study, FP1 had long algae filaments and exhibited a 310% increase in c_f, whereas FP2 was a low-form gelatinous biofilm and exhibited a 50% increase in c_f.

It is recognised that more detailed data is required. In future work, a Laser Doppler Velocimeter will be used to obtain detailed turbulence information to complement the current work using the floating element force balance and Pitot probes.

5 Conclusions

The growth of biofilms in hydroelectric canals and pipelines is a significant problem which extends to other industries. Boundary layer and total drag measurements on both smooth and fouled surfaces demonstrate that a fouled surface exhibits significantly greater drag than a smooth painted surface, and the magnitude of the drag depends on the physical nature of the biofilm. A 50-60% increase in drag was measured for a low-form gelatinous biofilm, and a 310% increase was measured for a biofilm consisting of long algae streamers and an underlying gelatinous biofilm.

6 Acknowledgments

This research project is funded by the Australian Research Council under the Linkage Projects Scheme, in partnership with Hydro Tasmania.

References:

[1] Lewthwaite, J., Molland, A. and Thomas, K., An Investigation into the Variation of Ship Skin Frictional Resistance with Fouling, *Trans. RINA*, 127, 1985, pp.269-284.

[2] Brett, T. M., Head-Loss Measurements on Hydroelectric Conduits, *ASCE J. Hydraulics Division*, HY1, 1980, pp.173- 190.

[3] Schultz, M. P. and Swain, G. W., The Effect of Biofilms on Turbulent Boundary Layers, *ASME J. Fluids Engineering*, 121, 1999, pp.44-51.

[4] Schultz, M. P., Turbulent Boundary Layers on Surfaces Covered with Filamentous Algae, *ASME J. Fluids Engineering*, 122, 2000, pp.357-363.

[5] Barton, A., Friction, Roughness and Boundary Layer Characteristics of Freshwater Biofilms in Hydraulic Conduits (PhD Thesis), 2006..

[6] Andrewartha, J., Sargison, J. and Perkins, K., The Effect of *Gomphonema* and Filamentous Algae Streamers on Hydroelectric Canal Capacity and Turbulent Boundary Layer Structure, *16th Australasian Fluid Mechanics Conference*, Gold Coast, Australia, 2007.

[7] Callow, M. E., A Review of Fouling in Freshwater, *Biofouling*, 7, 1993, pp.313-327.

[8] Wetherbee, R., Lind, J. L., Burke, J. and Quatrano, R. S., The First Kiss: Establishment and Control of Initial Adhesion by Raphid Diatoms, *J. Phycology*, 34, 1998, pp.9-15.

[9] Johnson, L., Hoagland, K. and Gretz, M., Effects of Bromide and Iodine on Stalk Secretion in the Biofouling Diatom Achnanthes Longipes (Bacillariophyceae), *J. Phycology*, 31, 1995, pp.401-412.

[10] Barton, A., Brandner, P., Sargison, J. and Walker, G., A Force Balance to Measure the Total Drag of Biofilms on Test Plates, *16th Australasian Fluid Mechanics Conference*, Gold Coast, Australia, 2007.

[11] Patel, V., Calibration of the Preston Tube and Limitations of its Use in Pressure Gradients, *J. Fluid Mechanics*, 23, 1, 1965, pp.185-208.

[12] McKeon, B., Li, J., Morrison, J. and Smits, A. J., Pitot Probe Corrections in Fully Developed Turbulent Pipe Flow, *Measurement Science and Technology*, 14, 2003, pp.1449-1458.

[13] Perry, A. E., Schofield, W. H. and Joubert, P. N., Rough Wall Turbulent Boundary Layers, *J. Fluid Mechanics*, 37, 2, 1969, pp.383-413.

[14] Schlichting, H., *Boundary Layer Theory*, Permagon Press Ltd, 1955.

[15] Coleman, H. and Steele, W., Engineering Application of Experimental Uncertainty Analysis, *AIAA Journal*, 33, 10, 1995, pp.1888-1895.

[16] Figliola, R. and Beasley, D., *Theory and Design for Mechanical Measurements*, John Wiley & Sons, 2000.